



Contents lists available at ScienceDirect



# Catalysis Today

journal homepage: [www.elsevier.com/locate/cattod](http://www.elsevier.com/locate/cattod)

## Gas-phase epoxidation of propylene by molecular oxygen over Ag/BaCO<sub>3</sub> catalysts: Effect of preparation conditions

Qing Zhang, Yanglong Guo\*, Wangcheng Zhan, Yun Guo, Li Wang, Yunsong Wang, Guanzhong Lu\*

Key Laboratory for Advanced Materials, Research Institute of Industrial Catalysis, East China University of Science and Technology, Shanghai 200237, PR China

### ARTICLE INFO

#### Article history:

Received 15 November 2015

Received in revised form

29 December 2015

Accepted 3 January 2016

Available online xxx

#### Keywords:

Epoxidation of propylene

Propylene oxide

Molecular oxygen

Ag/BaCO<sub>3</sub> catalyst

Ag crystallite size

### ABSTRACT

Ag/BaCO<sub>3</sub> catalysts with different Ag crystallite sizes, prepared by the reduction-deposition method, were developed for gas-phase epoxidation of propylene to propylene oxide (PO) by molecular oxygen. Effects of preparation conditions, such as pretreatment of organic amines of BaCO<sub>3</sub> support, pretreatment way of ethylene diamine, reduction temperature of HCHO and calcination temperature, on the catalytic performance and Ag crystallite size of Ag/BaCO<sub>3</sub> catalyst were investigated. Ag/BaCO<sub>3</sub>\* catalyst, with pretreatment of BaCO<sub>3</sub> support by ethylene diamine and prepared at the reduction temperature of HCHO of 10 °C and the calcination temperature of 250 °C, exhibited better catalytic performance and good durability, in which 12.5% of propylene conversion and 36.9% of PO selectivity were achieved under the reaction conditions of 20%C<sub>3</sub>H<sub>6</sub>–10%O<sub>2</sub>–70%N<sub>2</sub>, 200 °C, 0.1 MPa and GHSV of 3000 h<sup>-1</sup>. Both lower reduction temperature of HCHO and lower calcination temperature can get smaller Ag crystallite sizes, which is more effective for epoxidation of propylene over Ag/BaCO<sub>3</sub>\* catalyst. The catalytic reaction mechanism of Ag/BaCO<sub>3</sub>\* catalyst for epoxidation of propylene is that propylene in the gas phase reacts with molecular oxygen species adsorbed on the catalyst surface to produce PO and follows Rideal–Eley mechanism.

© 2016 Elsevier B.V. All rights reserved.

## 1. Introduction

Epoxidation of propylene to propylene oxide (PO) is one of the most important reactions in the chemical industry because PO is an important bulk chemical and widely used for production of propylene glycols, polyether polyols, polyurethane, surfactants and other commercial products. PO is produced mainly by the chlorohydrin process, the Halcon process and the hydroperoxide process, however, which have several shortcomings. The chlorohydrin process is not environmentally friendly and produces a large number of chlorinated by-products. The Halcon process generates the equimolar coproducts which values depend on their demands in the market [1]. The hydroperoxide process needs construction of large-scale production equipments and its commercialization has been hindered largely by the expense of H<sub>2</sub>O<sub>2</sub> [2]. The Au-based catalysts can produce PO from epoxidation of propylene by the in-situ production of H<sub>2</sub>O<sub>2</sub> from H<sub>2</sub>–O<sub>2</sub> mixture with a high selectivity [3–10]. However, H<sub>2</sub> must be used as a sacrificial coreactant and its effi-

ciency is usually low. Gas-phase epoxidation of propylene to PO by molecular oxygen is a one-step green chemical process, which has attracted much attention in recent years. Ag nanoparticles of 2–5 nm supported on WO<sub>3</sub> nanorods could get 15.5% of propylene conversion with 83% of PO selectivity [11]. Dissociation of O<sub>2</sub> at the interface between Ag aggregates and Al<sub>2</sub>O<sub>3</sub> support could account for high catalytic activity for epoxidation of propylene over Ag<sub>19</sub>/Al<sub>2</sub>O<sub>3</sub> catalyst [12]. TiCuO<sub>x</sub> mixed oxide catalyst with highly dispersed and stabilized active sites of Cu<sup>+</sup> could get 69% of PO selectivity [13]. A strong synergistic effect between CuO<sub>x</sub> and RuO<sub>x</sub> was found to be responsible for PO formation over RuO<sub>x</sub>–CuO<sub>x</sub>/SiO<sub>2</sub> catalyst [14]. SnO<sub>2</sub>–CuO–NaCl/SiO<sub>2</sub> catalyst [15] and NaCl–Cu–Mn mixed metal oxide catalyst [16] were also found to be effective for epoxidation of propylene by molecular oxygen. Strong interaction between Cs<sup>+</sup> and CuO<sub>x</sub> nanoparticles favored the selective formation of PO over Cs<sup>+</sup>–CuO<sub>x</sub>/SiO<sub>2</sub> catalyst [17] and Cu<sup>+</sup> was thought to be active sites for PO formation [17,18]. The light-induced reduction of Cu catalysts could increase PO selectivity [19] and Cu<sub>2</sub>O rhombic dodecahedra exposing (111) crystal planes were found to be most effective for PO formation among Cu<sub>2</sub>O catalysts with different morphologies [20]. The unsupported AgCu bimetallic catalyst

\* Corresponding authors. Fax: +86 21 64252923.

E-mail addresses: [yguo@ecust.edu.cn](mailto:yguo@ecust.edu.cn) (Y. Guo), [gzhlu@ecust.edu.cn](mailto:gzhlu@ecust.edu.cn) (G. Lu).

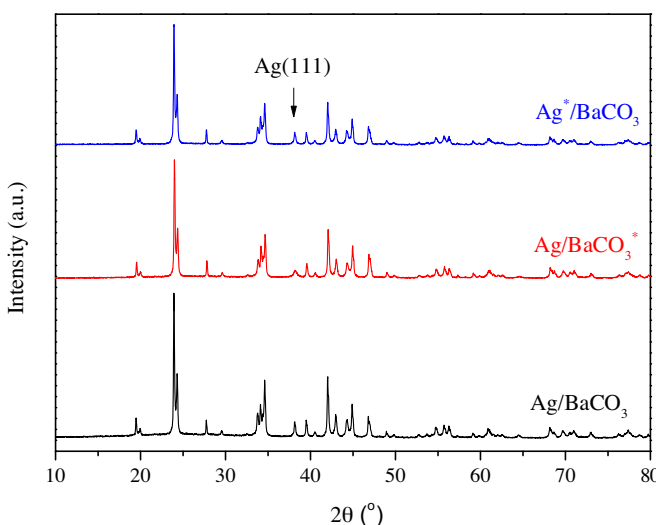


**Fig. 1.** XRD patterns of  $\text{Ag}/\text{BaCO}_3$ ,  $\text{Ag}/\text{BaCO}_3^*$  and  $\text{Ag}^*/\text{BaCO}_3$  catalysts.

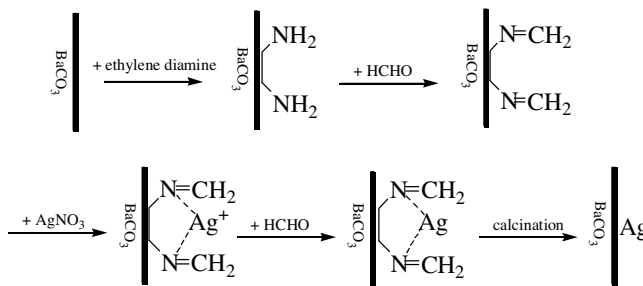


**Fig. 2.** Schematic diagram of the preparation process of  $\text{Ag}/\text{BaCO}_3^*$  catalyst.

was more stable than unsupported Cu catalyst for epoxidation of propylene [21].

Epoxidation of ethylene by molecular oxygen over Ag-based catalysts has been commercialized for several decades, in which 83–95% of selectivity of ethylene oxide is obtained [22–24]. Ag-based catalysts have also been investigated for epoxidation of propylene by molecular oxygen. However, PO selectivity is low over unpromoted Ag catalysts, because propylene has the active  $\alpha$ -H atoms and  $\alpha$ -H atoms can easily react with oxygen to result in combustion of propylene to  $\text{CO}_2$  and  $\text{H}_2\text{O}$ . Therefore, various attempts have been made to modify Ag catalysts for epoxidation of propylene.  $\text{NaCl}$ ,  $\text{CuCl}$ ,  $\text{Y}_2\text{O}_3$ ,  $\text{K}_2\text{O}$  and  $\text{MoO}_3$  have been used as promoters to enhance PO selectivity [25–30]. These Ag-based catalysts were effective for epoxidation of propylene, but they were high Ag loading or heavily promoted.  $\text{Ag}/\text{Cu}$  bimetallic catalyst with low loadings of Ag and Cu, could get PO selectivity of 55.1% at propylene conversion of 3.6% [31].

Gas-phase epoxidation of propylene by molecular oxygen over Ag-based catalysts is a structure-sensitive reaction, but opinions are different. Zemichael et al. [27] found that  $\text{Ag}/\text{CaCO}_3$  catalyst with Ag nanoparticles of 20–40 nm exhibited better catalytic performance. Lu et al. [32] showed that large Ag nanoparticles favored ethylene epoxidation by 3–5 fold at 473–493 K, whereas Ag particle size did not have a large effect on propylene epoxidation over  $\text{Ag}/\text{CaCO}_3$  catalyst. Molina et al. [33] found that  $\text{Ag}/\text{Al}_2\text{O}_3$  catalyst with Ag nanoparticles of 23.3 nm was more selective towards PO formation. Lei et al. [34] found that size-selected  $\text{Ag}_3$  clusters and Ag nanoparticles of  $\sim 3.5$  nm on alumina supports could catalyze epoxidation of propylene by molecular oxygen with high PO selectivity at low temperature. Ghosh et al. [11] found that  $\text{Ag}/\text{WO}_3$  catalyst with 2–5 nm Ag particle size was much more effective than those

with 15–20 nm or 30–50 nm Ag particle size for epoxidation of propylene by molecular oxygen at high pressure. DFT calculations showed that  $\text{CO}_2$  was the main product for epoxidation of propylene by  $\text{O}_2$  or  $\text{H}_2-\text{O}_2$  mixtures irrespective of the silver particle size [35].

In this paper, unpromoted  $\text{Ag}/\text{BaCO}_3$  catalysts with low Ag loading were prepared by the reduction-deposition method and investigated for gas-phase epoxidation of propylene by molecular oxygen at atmospheric pressure. Effects of preparation conditions, such as pretreatment of organic amines of  $\text{BaCO}_3$  support, pretreatment way of ethylene diamine, calcination temperature and reduction temperature of  $\text{HCHO}$ , on the catalytic performance and Ag crystallite size of  $\text{Ag}/\text{BaCO}_3$  catalyst were investigated, and the catalytic reaction mechanism for epoxidation of propylene was proposed.

## 2. Experimental

### 2.1. Preparation of catalysts

$\text{Ag}/\text{BaCO}_3$  catalyst was prepared by the reduction-deposition method. At room temperature, 2 g of formaldehyde ( $\text{HCHO}$ ) was dissolved in 40 mL of deionized water as the reductant, into which 8 g of  $\text{BaCO}_3$  support was added to form a slurry. After stirring for 20 min, 0.6 g of  $\text{AgNO}_3$  dissolved in 40 mL of deionized water was added dropwise into the above slurry, then the solid was filtered and washed with deionized water and ethanol for several times. The solid was dried overnight at room temperature and then calcined in  $\text{N}_2$  atmosphere at 450 °C for 4 h. The similar procedure was used to prepare  $\text{Ag}^*/\text{BaCO}_3$  catalyst except that  $\text{AgNO}_3$  was firstly dissolved in deionized water and then ethylene diamine was added until the solution became clear.  $\text{Ag}/\text{BaCO}_3^*$  catalyst was prepared by the similar method to  $\text{Ag}/\text{BaCO}_3$  catalyst except that  $\text{BaCO}_3$  support was firstly immersed into ethylene diamine aqueous solution for 12 h and then dried under vacuum at 60 °C for 4.5 h.

### 2.2. Epoxidation of propylene

Epoxidation of propylene was carried out in a fixed-bed quartz reactor under the reaction conditions of 0.6 g catalyst, 200 °C, 0.1 MPa and GHSV of 3000  $\text{h}^{-1}$ . The feed gas consisted of 20% propylene, 10%  $\text{O}_2$  and balance  $\text{N}_2$ . Reaction products were analyzed by two on-line gas chromatographs equipped with a two packed columns (G.D.X-401 and Porapak Q) with FID and TCD detectors. All lines between the reactor exit and the gas chromatographs were heated to 120 °C to prevent condensation of the products. PO selectivity and propylene conversion were calculated on a carbon balance basis.

### 2.3. Characterization of catalysts

Elemental analysis was done by inductively coupled-plasma atomic emission spectroscopy (ICP-AES) using a TJA IRIS ADVANTAGE 1000 instrument.

XRD patterns were performed on a Bruker AXS D8 Focus diffractometer operated at 40 kV, 40 mA ( $\text{Cu K}\alpha$  radiation,  $\lambda = 0.15406 \text{ nm}$ ).

TEM images were recorded on a JEM-1400 transmission electron microscope. The sample was ultrasonically suspended in the ethanol solvent, and one drop of this slurry was deposited on a copper grid. The liquid phase was evaporated before the grid was loaded into the microscope.

XPS spectra were recorded on a Thermo ESCALAB 250 spectrometer with a monochromatized  $\text{AlK}\alpha$  X-ray source (1486.6 eV), and a passing energy of 20 eV. C1s (binding energy of 284.6 eV) of adventitious carbon was used as the reference.

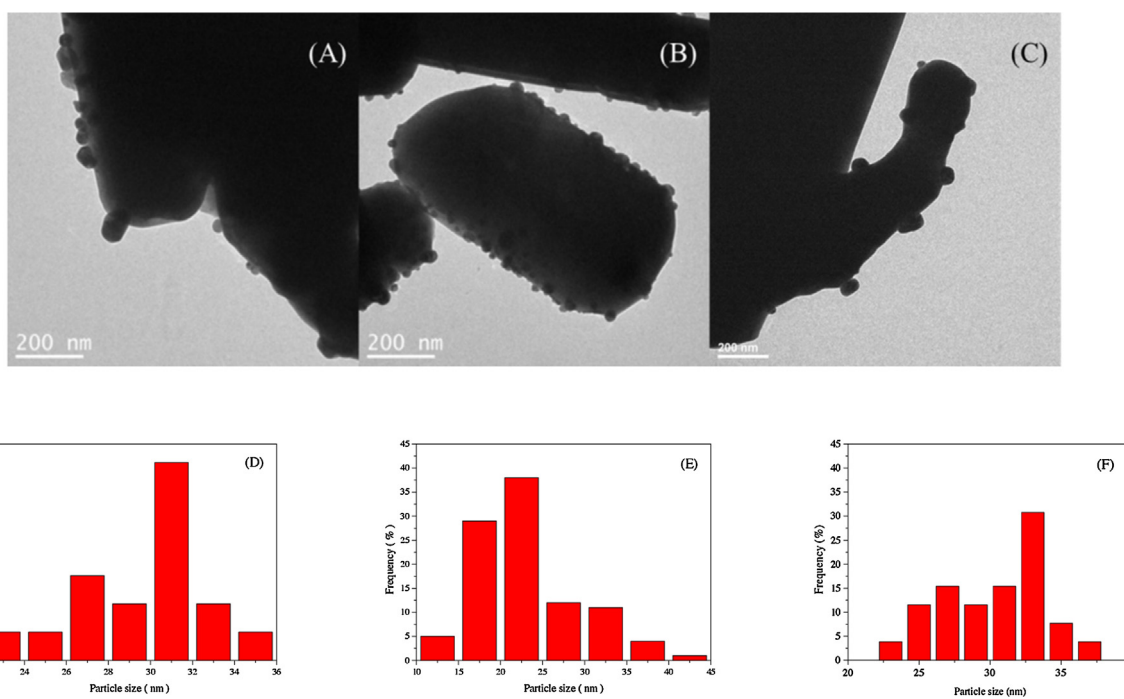


**Fig. 3.** TEM images and the corresponding Ag particle size distribution histograms of Ag/BaCO<sub>3</sub> (A) (D), Ag/BaCO<sub>3</sub><sup>\*</sup> (B) (E), Ag\*/BaCO<sub>3</sub> catalysts (C) (F).

Temperature programmed desorption of O<sub>2</sub> (O<sub>2</sub>-TPD) and C<sub>3</sub>H<sub>6</sub> (C<sub>3</sub>H<sub>6</sub>-TPD) and temperature programmed oxidation of O<sub>2</sub> (O<sub>2</sub>-TPO) were carried out on a Micromeritics AutoChem 2920 II chemisorption analyzer with a Hiden HPR 20 mass spectrometer. For O<sub>2</sub>-TPD and C<sub>3</sub>H<sub>6</sub>-TPD, 500 mg samples of 40–60 mesh were loaded in a quartz reactor and pretreated in a He flow of 30 mL min<sup>-1</sup> at 250 °C for 0.5 h. After it was cooled down to room temperature, a gas flow of O<sub>2</sub>-He (3 vol. % O<sub>2</sub>) or a gas flow of C<sub>3</sub>H<sub>6</sub>-Ar (1 vol. % C<sub>3</sub>H<sub>6</sub>) of 20 mL min<sup>-1</sup> was introduced into the reactor, the reactor temperature was raised to 200 °C at a rate of 10 °C min<sup>-1</sup> and was kept at 200 °C for 0.5 h, then cooled down to room temperature. After that, a He flow of 20 mL min<sup>-1</sup> was switched. When the baseline was stable, the reactor temperature was raised to 600 °C at a heating rate of 10 °C min<sup>-1</sup>. The MS signals of O<sub>2</sub> (*m/z*=32) or C<sub>3</sub>H<sub>6</sub> (*m/z*=41) were recorded by the mass spectrometer. For O<sub>2</sub>-TPO experiment, a gas flow of O<sub>2</sub>-He (3 vol. % O<sub>2</sub>) of 10 mL min<sup>-1</sup> was introduced into the quartz reactor loaded with 500 mg samples of 40–60 mesh. The reactor temperature was raised to 250 °C at a heating rate of 10 °C min<sup>-1</sup>. The MS signals of CO<sub>2</sub> (*m/e*=44) and H<sub>2</sub>O (*m/e*=18) were recorded.

### 3. Results and discussion

#### 3.1. Catalytic performance of catalysts

**Table 1** shows effect of the pretreatment of different organic amines of BaCO<sub>3</sub> supports on the catalytic performance of Ag/BaCO<sub>3</sub><sup>\*</sup> catalysts for gas-phase epoxidation of propylene by molecular oxygen. As shown in **Table 1**, the pretreatment of organic amines except for ethylene diamine of BaCO<sub>3</sub> supports decreased both propylene conversion and PO selectivity compared with Ag/BaCO<sub>3</sub> catalyst. When BaCO<sub>3</sub> support was pretreated with ethylene diamine, the catalytic performance of Ag/BaCO<sub>3</sub><sup>\*</sup> catalyst was better than that of Ag/BaCO<sub>3</sub> catalyst, in which propylene conversion increased dramatically from 1.5% to 8.1%, and PO selectivity increased obviously from 22.8% to 31.9%. Then, we investigated effect of the pretreatment way of ethylene diamine on the catalytic performance of Ag/BaCO<sub>3</sub> catalysts, which is shown in **Table 2**.

As shown in **Table 2**, Ag loadings of Ag/BaCO<sub>3</sub>, Ag/BaCO<sub>3</sub><sup>\*</sup> and Ag\*/BaCO<sub>3</sub> catalysts were at the similar values of 4.0 wt.%, 4.3 wt.% and 4.3 wt.%, respectively. However, the catalytic performance of these three catalysts varied considerably. When AgNO<sub>3</sub> reacted with ethylene diamine to form a complex and then reduced by HCHO, the catalytic performance of Ag\*/BaCO<sub>3</sub> catalyst was not improved compared with Ag/BaCO<sub>3</sub> catalyst, in which propylene conversion and PO selectivity were 1.0% and 24.2%, respectively.

#### 3.2. XRD

**Fig. 1** shows XRD patterns of Ag/BaCO<sub>3</sub>, Ag/BaCO<sub>3</sub><sup>\*</sup> and Ag\*/BaCO<sub>3</sub> catalysts. As shown in **Fig. 1**, over these three catalysts, only the characteristic diffraction peak of Ag (111) at  $2\theta=38.1^\circ$  and the diffraction peaks of BaCO<sub>3</sub> support were observed, which was similar to Ag-Cu/BaCO<sub>3</sub> catalyst [31]. Ag crystallite size was determined by Scherrer's equation with the full peak width at half maximum height of the diffraction peak of Ag (111) from XRD patterns. As shown in **Table 2**, Ag crystallite sizes of Ag/BaCO<sub>3</sub>, Ag\*/BaCO<sub>3</sub> and Ag/BaCO<sub>3</sub><sup>\*</sup> catalysts were about 29 nm, 31 nm and 20 nm, respectively, which indicated that when BaCO<sub>3</sub> support was pretreated with ethylene diamine, Ag/BaCO<sub>3</sub><sup>\*</sup> catalyst could get much smaller Ag crystallite size. The schematic diagram of the preparation process of Ag/BaCO<sub>3</sub><sup>\*</sup> catalyst was proposed in **Fig. 2**. The pretreatment of BaCO<sub>3</sub> support with ethylene diamine made BaCO<sub>3</sub> support functionalized with amine groups. When BaCO<sub>3</sub> support functionalized with amine groups was added into HCHO aqueous solution, amine groups reacted with HCHO to form a Schiff base (the N=CH<sub>2</sub> group) which had a strong complexation with Ag<sup>+</sup> due to metal to ligand back-bonding benefit for immobilization and localization of Ag<sup>+</sup> on the surface of BaCO<sub>3</sub> support [36]. Then, the excess HCHO reduced the complex to form Ag nanoparticles deposited on the surface of BaCO<sub>3</sub> support, leading to high dispersion of Ag nanoparticles with smaller Ag crystallite size. In this preparation process, functionalization of BaCO<sub>3</sub> support with ethylene diamine was very important for anchoring Ag nanoparticles due to the strong interaction between them. Yu et al. [36] prepared the ultrasmall Ag nanoparticles based on the introduction of the

**Table 1**

Effect of the pretreatment of different organic amines of  $\text{BaCO}_3$  supports on the catalytic performance of  $\text{Ag}/\text{BaCO}_3^*$  catalysts.

Organic amines	Propylene conversion (%)	PO selectivity (%)	$\text{CO}_2$ selectivity (%)
Blank	1.5	22.8	77.2
Diethylamine	0.6	21.0	79.0
Triethylamine	0.8	20.5	79.5
n-Butylamine	0.6	23.0	77.0
Ethylene diamine	8.1	31.9	68.1
1,6-Hexamethylene diamine	1.5	1.6	98.4
Triethylenetetramine	0.9	19.6	80.4

Reaction conditions: 0.6 g catalyst, 20%  $\text{C}_3\text{H}_6$ –10%  $\text{O}_2$ –70%  $\text{N}_2$ , 200 °C, 0.1 MPa, 3000 h<sup>-1</sup>.

**Table 2**

Effect of the pretreatment way of ethylene diamine on the catalytic performance of  $\text{Ag}/\text{BaCO}_3$  catalysts.

Catalysts	Ag loading (wt.%) <sup>a</sup>	Propylene conversion (%)	PO selectivity (%)	Ag crystallite size (nm) <sup>b</sup>	Ag particle size (nm) <sup>c</sup>
$\text{Ag}/\text{BaCO}_3$	4.0	1.5	22.8	29	30
$\text{Ag}/\text{BaCO}_3^*$	4.3	8.1	31.9	20	20
$\text{Ag}^*/\text{BaCO}_3$	4.3	1.0	24.2	31	32

Reaction conditions: 0.6 g catalyst, 20%  $\text{C}_3\text{H}_6$ –10%  $\text{O}_2$ –70%  $\text{N}_2$ , 200 °C, 0.1 MPa, 3000 h<sup>-1</sup>.

<sup>a</sup> Measured by ICP-AES.

<sup>b</sup> Determined from XRD patterns by Scherrer's equation.

<sup>c</sup> Determined from particle size distribution histograms.

functional monomer salicylaldimine Schiff base into a  $\text{SiO}_2$  matrix. Yang et al. [37] prepared Pt–Ru nanoparticles dispersed uniformly on the ethylene diamine-grafted CNTs. Wang et al. [38] developed a two-step method including functionalization of the support with amine groups for synthesis of Au–Ag alloy, which proved effective in producing uniform bimetallic nanoparticles.

$\text{Ag}/\text{BaCO}_3^*$  catalyst with smaller Ag crystallite size got higher propylene conversion and higher PO selectivity than  $\text{Ag}/\text{BaCO}_3$  catalyst, which indicated that smaller Ag crystallite size was more effective for epoxidation of propylene by molecular oxygen.

### 3.3. TEM

Fig. 3 shows TEM images and Ag particle size distribution histograms of  $\text{Ag}/\text{BaCO}_3$ ,  $\text{Ag}/\text{BaCO}_3^*$  and  $\text{Ag}^*/\text{BaCO}_3$  catalysts. As shown in Fig. 3, spherical-like Ag nanoparticles were supported on the surface of bar-like  $\text{BaCO}_3$  supports. The number of Ag nanoparticles on the surface of  $\text{Ag}/\text{BaCO}_3^*$  catalyst was greater than those of  $\text{Ag}/\text{BaCO}_3$  and  $\text{Ag}^*/\text{BaCO}_3$  catalysts, and Ag particle size of  $\text{Ag}/\text{BaCO}_3^*$  catalyst was much smaller than those of  $\text{Ag}/\text{BaCO}_3$  and  $\text{Ag}^*/\text{BaCO}_3$  catalysts. These three catalysts had a wide distribution of Ag particle size probably because of the preparation method and the low surface area of  $\text{BaCO}_3$  support of 5 m<sup>2</sup> g<sup>-1</sup>. The particle size of most of Ag nanoparticles of  $\text{Ag}/\text{BaCO}_3$  and  $\text{Ag}^*/\text{BaCO}_3$  catalysts were from 30 nm to 32 nm, and the particle size of most of Ag nanoparticles of  $\text{Ag}/\text{BaCO}_3^*$  catalyst was about 20 nm, which were consistent with the results of XRD characterization.

### 3.4. XPS

Fig. 4 shows Ag3d XPS spectra of  $\text{Ag}/\text{BaCO}_3$ ,  $\text{Ag}/\text{BaCO}_3^*$  and  $\text{Ag}^*/\text{BaCO}_3$  catalysts. The binding energies of  $\text{Ag}3d_{3/2}$  and  $\text{Ag}3d_{5/2}$  of  $\text{Ag}/\text{BaCO}_3$ ,  $\text{Ag}/\text{BaCO}_3^*$  and  $\text{Ag}^*/\text{BaCO}_3$  catalysts were at the same values of 374.3 eV and 368.3 eV, respectively, which were attributed to  $\text{Ag}^\circ$ . This indicated the formation of metal state of silver nanoparticles on the surface of  $\text{BaCO}_3$  support in consistent with TEM images. At the same time, N element on the surface of  $\text{BaCO}_3$  support was not detected in the XPS spectra, which implied that ethylene diamine just played its role in the preparation process of the catalyst and then decomposed during the calcination process.

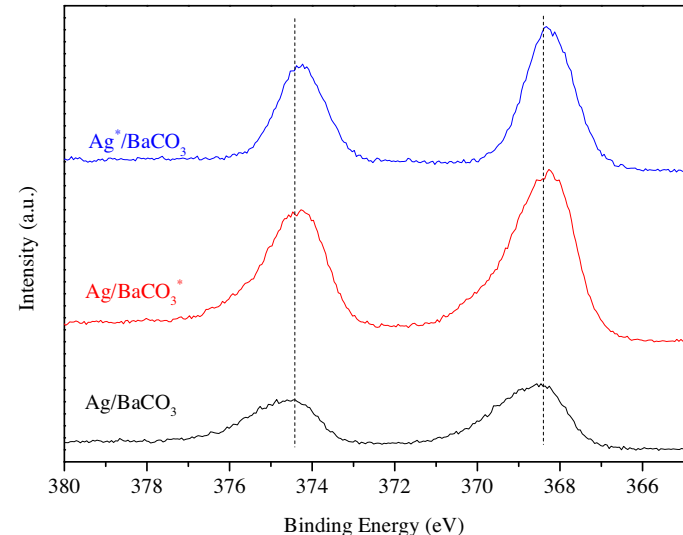
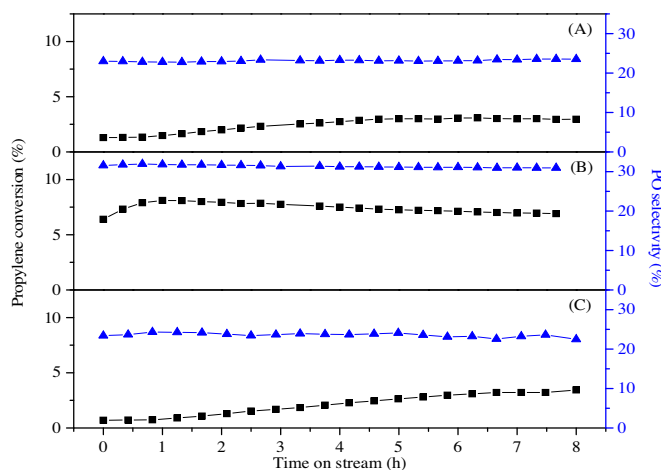


Fig. 4. Ag3d XPS spectra of  $\text{Ag}/\text{BaCO}_3$ ,  $\text{Ag}/\text{BaCO}_3^*$  and  $\text{Ag}^*/\text{BaCO}_3$  catalysts.

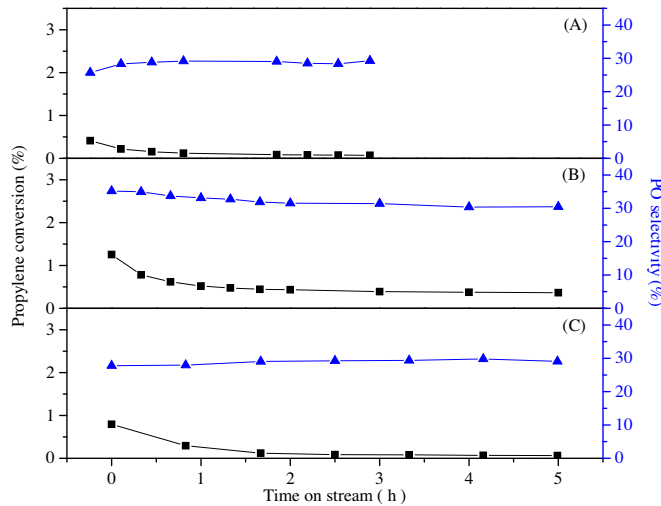
### 3.5. Stability of catalysts

Fig. 5 and Fig. 6 show the stability of  $\text{Ag}/\text{BaCO}_3$ ,  $\text{Ag}/\text{BaCO}_3^*$  and  $\text{Ag}^*/\text{BaCO}_3$  catalysts for epoxidation of propylene by molecular oxygen at the reaction temperatures of 200 °C and 160 °C, respectively. As shown in Fig. 5, for these three catalysts at the reaction temperature of 200 °C, with an increase in time on stream, PO selectivity kept nearly the same values, while propylene conversion changed a little firstly and then remained steady, which implied that there was an induction period for the epoxidation reaction. For  $\text{Ag}/\text{BaCO}_3$  and  $\text{Ag}^*/\text{BaCO}_3$  catalysts, propylene conversion increased gradually and then reached at 2.9% and 3.4%, respectively, after reaction for 8 h. For  $\text{Ag}/\text{BaCO}_3^*$  catalyst, propylene conversion increased from 6.3% to 8.1% at the first hour and then decreased a little. Propylene conversion of 7.2% and PO selectivity of 31% were achieved after reaction for 8 h over  $\text{Ag}/\text{BaCO}_3^*$  catalyst. Therefore  $\text{Ag}/\text{BaCO}_3$ ,  $\text{Ag}/\text{BaCO}_3^*$  and  $\text{Ag}^*/\text{BaCO}_3$  catalysts exhibited good durability for epoxidation of propylene at the reaction temperature of 200 °C.

However, as shown in Fig. 6, the stability of these three catalysts at the reaction temperature of 160 °C was totally different from the stability at the reaction temperature of 200 °C shown in



**Fig. 5.** The catalyst stability for epoxidation of propylene over Ag/BaCO<sub>3</sub> catalyst (A), Ag/BaCO<sub>3</sub><sup>\*</sup> catalyst (B) and Ag<sup>\*</sup>/BaCO<sub>3</sub> catalyst (C). Reaction conditions: 0.6 g catalyst, 20% C<sub>3</sub>H<sub>6</sub>–10% O<sub>2</sub>–70% N<sub>2</sub>, 200 °C, 0.1 MPa, 3000 h<sup>-1</sup>.



**Fig. 6.** The catalyst stability for epoxidation of propylene over Ag/BaCO<sub>3</sub> catalyst (A), Ag/BaCO<sub>3</sub><sup>\*</sup> catalyst (B), Ag<sup>\*</sup>/BaCO<sub>3</sub> catalyst (C). Reaction conditions: 0.6 g catalyst, 20% C<sub>3</sub>H<sub>6</sub>–10% O<sub>2</sub>–70% N<sub>2</sub>, 160 °C, 0.1 MPa, 3000 h<sup>-1</sup>.

**Fig. 5.** With an increase in time on stream, PO selectivity kept almost the same values, but propylene conversion decreased significantly. After reaction for several hours, propylene conversion decreased to nearly 0 over Ag/BaCO<sub>3</sub> and Ag<sup>\*</sup>/BaCO<sub>3</sub> catalysts and to 0.4% over Ag/BaCO<sub>3</sub><sup>\*</sup> catalyst, which indicated that these three catalysts were easily deactivated at low temperature due to coke deposition.

O<sub>2</sub>-TPO characterization was performed to demonstrate whether coke deposition led to deactivation of Ag/BaCO<sub>3</sub>, Ag/BaCO<sub>3</sub><sup>\*</sup> and Ag<sup>\*</sup>/BaCO<sub>3</sub> catalysts for epoxidation of propylene at the reaction temperature of 160 °C, which is shown in Fig. 7. The MS peaks of CO<sub>2</sub> (*m/z* = 44) and H<sub>2</sub>O (*m/z* = 18) were observed at the same temperatures, which demonstrated that carbonaceous species on the surface of the deactivated catalysts were oxidized. The MS peaks of CO<sub>2</sub> and H<sub>2</sub>O of the deactivated Ag/BaCO<sub>3</sub><sup>\*</sup> catalyst were observed at about 170 °C, while the peaks of CO<sub>2</sub> and H<sub>2</sub>O of the deactivated Ag/BaCO<sub>3</sub> and Ag<sup>\*</sup>/BaCO<sub>3</sub> catalysts were observed at about 190 °C. Carbonaceous species could be oxidized to CO<sub>2</sub> and H<sub>2</sub>O at lower temperature over the deactivated Ag/BaCO<sub>3</sub><sup>\*</sup> catalyst with smaller Ag crystallite size. Bhavani et al. [39] investigated how the metal Ni particle size influenced the coke formation over Ni-M/AlCeZrO<sub>x</sub> bimetallic catalysts for the oxidative CO<sub>2</sub> reforming of CH<sub>4</sub>, in which coke deposition was much easier to react with oxygen over the catalyst with smaller Ni particle size.

### 3.6. Effect of Ag crystallite size

#### 3.6.1. Effect of calcination temperature

Smaller Ag crystallite sizes could get higher propylene conversion and higher PO selectivity, comparing Ag/BaCO<sub>3</sub>, Ag/BaCO<sub>3</sub><sup>\*</sup> and Ag<sup>\*</sup>/BaCO<sub>3</sub> catalysts. In order to further optimize the catalytic performance of Ag/BaCO<sub>3</sub><sup>\*</sup> catalyst for epoxidation of propylene, experiments were performed to investigate effect of Ag crystallite size by changing preparation parameters.

Thermal treatment is a simple and efficient way to control the crystallite size of metal catalysts. Sintering and aggregation of Ag nanoparticles happened more or less with the calcination temperature over 200 °C [40]. Fig. 8 shows effect of the calcination temperature on the catalytic performance of Ag/BaCO<sub>3</sub><sup>\*</sup> catalyst for epoxidation of propylene. As shown in Fig. 8, the calcination temperature had a significant effect on propylene conversion but little effect on PO selectivity over Ag/BaCO<sub>3</sub><sup>\*</sup> catalyst. When the calcination temperature increased from 250 °C to 650 °C, propylene conversion decreased greatly from 9.5% to 2.7%, and PO selectivity decreased gradually from 33.7% to 29.9%.

Fig. 9 shows XRD patterns of Ag/BaCO<sub>3</sub><sup>\*</sup> catalysts with different calcination temperatures. The diffraction peak of Ag (111) at

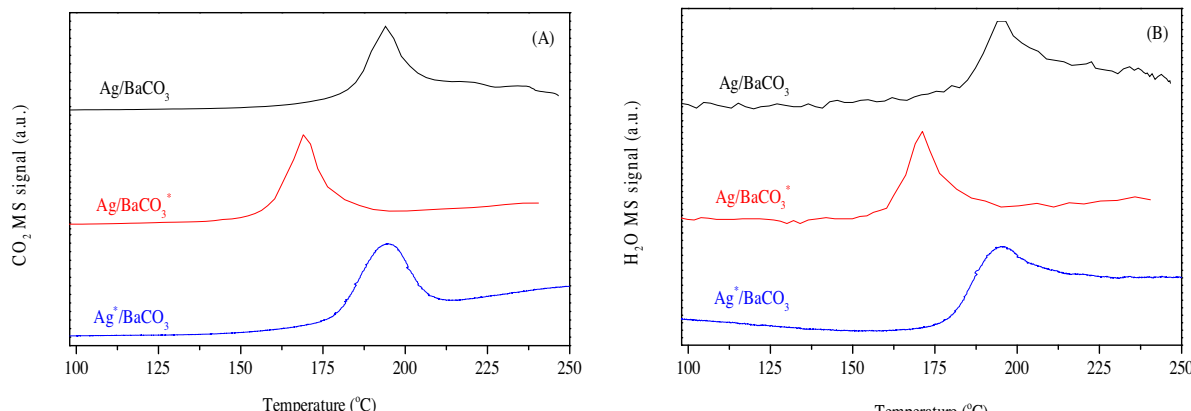


**Fig. 7.** O<sub>2</sub>-TPO profiles of the deactivated catalysts for epoxidation of propylene at the reaction temperature of 160 °C: (A) CO<sub>2</sub> MS signal (*m/z* = 44), (B) H<sub>2</sub>O MS signal (*m/z* = 18).

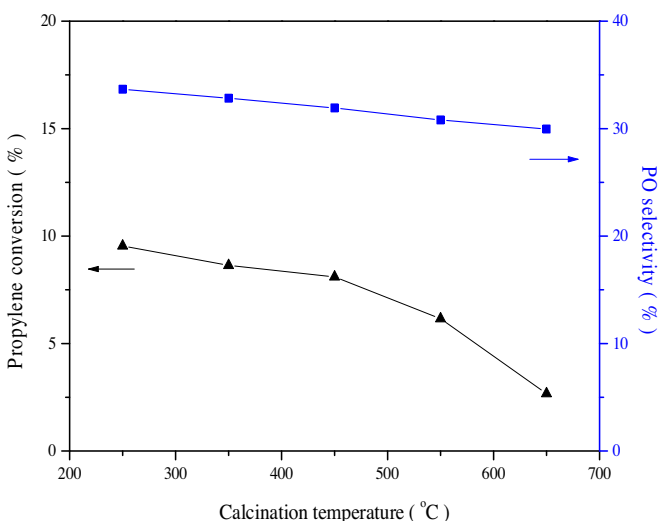


**Fig. 8.** Effect of the calcination temperature on the catalytic performance of  $\text{Ag}/\text{BaCO}_3^*$  catalyst for epoxidation of propylene.

Reaction conditions: 0.6 g catalyst, 20%  $\text{C}_3\text{H}_6$ -10%  $\text{O}_2$ -70%  $\text{N}_2$ , 200 °C, 0.1 MPa, 3000 h<sup>-1</sup>.

$2\theta = 38.1^\circ$  became much sharper with increasing the calcination temperature. Ag crystallite size, determined by Scherrer's equation, grew from about 20 nm at the calcination temperature of 250 °C to about 34 nm at the calcination temperature of 650 °C. Metal catalysts usually sinter and aggregate seriously at high temperatures [41,42], however, Ag nanoparticles of  $\text{Ag}/\text{BaCO}_3^*$  catalyst didn't grow much, which indicated that  $\text{Ag}/\text{BaCO}_3^*$  catalyst had a good thermostability. Therefore both propylene conversion and PO selectivity decreased with the growth of Ag crystallite size of  $\text{Ag}/\text{BaCO}_3^*$  catalyst by increasing the calcination temperature.

### 3.6.2. Effect of reduction temperature of HCHO

$\text{Ag}/\text{BaCO}_3^*$  catalyst with smaller Ag crystallite sizes at lower calcination temperature could get better catalytic performance for epoxidation of propylene, therefore we chose 250 °C as the calcination temperature in the following researches.

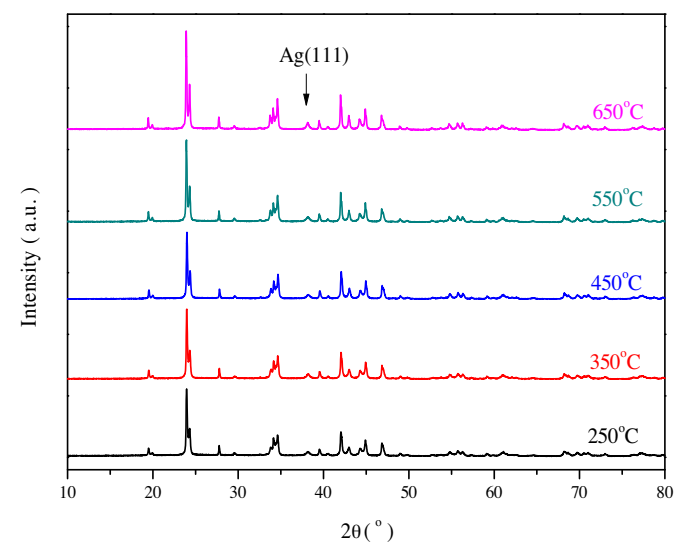


**Fig. 9.** XRD patterns of  $\text{Ag}/\text{BaCO}_3^*$  catalysts with different calcination temperatures.

**Fig. 10** shows effect of the reduction temperature of HCHO on the catalytic performance of  $\text{Ag}/\text{BaCO}_3^*$  catalyst for epoxidation of propylene. These four catalysts with different reduction temperature of HCHO were calcined at 250 °C in  $\text{N}_2$  atmosphere. As shown in **Fig. 10**, the reduction temperature of HCHO had a great effect on the catalytic performance of  $\text{Ag}/\text{BaCO}_3^*$  catalyst. With the reduction temperature of HCHO increasing from 10 °C to 50 °C, propylene conversion decreased significantly from 12.5% to 1.6%, and PO selectivity decreased greatly from 36.9% to 16.5%.

**Fig. 11** shows XRD patterns of  $\text{Ag}/\text{BaCO}_3^*$  catalysts with different reduction temperatures of HCHO. The diffraction peak of Ag (111) at  $2\theta = 38.1^\circ$  became much sharper with increasing the reduction temperature of HCHO. Ag crystallite size, determined by Scherrer's equation, grew from about 18 nm at the reduction temperature of HCHO of 10 °C to about 40 nm at the reduction temperature of HCHO of 50 °C. The reasons for the growth of Ag crystallite size were as follows. With increasing the reduction tem-

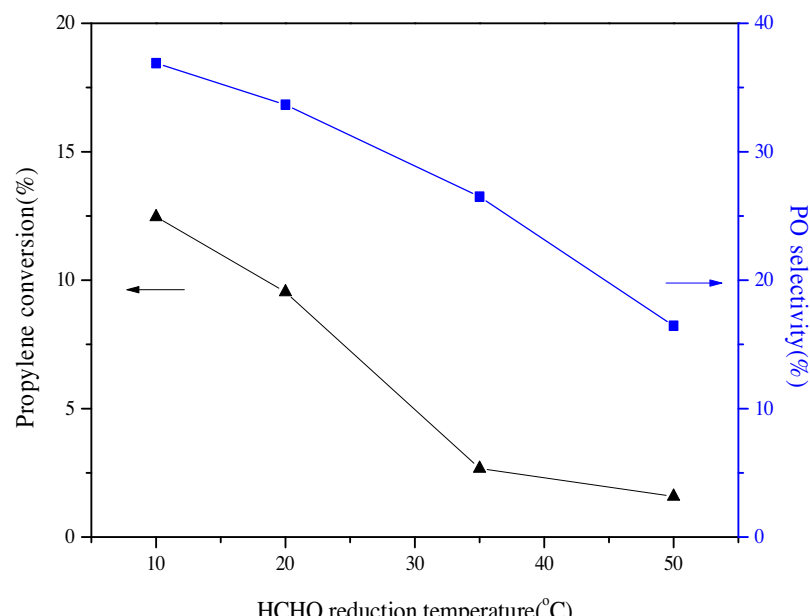


**Fig. 10.** Effect of reduction temperature of HCHO on the catalytic performance of  $\text{Ag}/\text{BaCO}_3^*$  catalyst for epoxidation of propylene.

Reaction conditions: 0.6 g catalyst, 20%  $\text{C}_3\text{H}_6$ -10%  $\text{O}_2$ -70%  $\text{N}_2$ , 200 °C, 0.1 MPa, 3000 h<sup>-1</sup>.

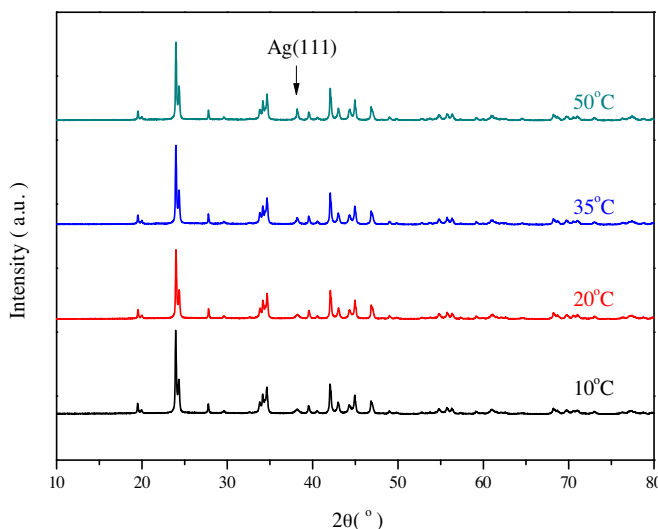


**Fig. 11.** XRD patterns of  $\text{Ag}/\text{BaCO}_3^*$  catalysts with different reduction temperatures of HCHO.

perature of HCHO, the reducing power of HCHO became stronger and then led to faster reduction of Ag cations to larger Ag nanoparticles. Moreover, at higher reduction temperature of HCHO, Ag nanoparticles aggregated faster. Therefore both propylene conversion and PO selectivity decreased with the growth of Ag crystallite size of  $\text{Ag}/\text{BaCO}_3^*$  catalyst by increasing the reduction temperature of HCHO.

Both lower calcination temperature and lower reduction temperature of HCHO can get smaller Ag crystallite sizes, which is more effective for epoxidation of propylene by molecular oxygen over  $\text{Ag}/\text{BaCO}_3^*$  catalyst.  $\text{Ag}/\text{BaCO}_3^*$  catalyst with the Ag crystallite size of about 18 nm, prepared at the reduction temperature of HCHO of 10 °C and the calcination temperature of 250 °C in  $\text{N}_2$  atmosphere, achieved 12.5% of propylene conversion and 36.9% of PO selectivity at the reaction temperature of 200 °C. Although  $\text{Ag}/\text{WO}_3$  catalyst could achieve 15.5% of propylene conversion and 83% of PO selectivity for epoxidation of propylene by molecular oxygen at high reaction pressure of 2 MPa and 250 °C,  $\text{Ag}/\text{WO}_3$  catalyst only achieved 3% of propylene conversion and 27% of PO selectivity at 0.1 MPa and 250 °C [11], which is much worse than the catalytic performance of  $\text{Ag}/\text{BaCO}_3^*$  catalyst in this work. Unfortunately,  $\text{Ag}/\text{BaCO}_3^*$  catalyst with Ag crystallite size smaller than 18 nm couldn't be prepared in this work because of the low surface area of  $\text{BaCO}_3$  support of  $5 \text{ m}^2 \text{ g}^{-1}$ . Therefore smaller Ag crystallite size is more effective for epoxidation of propylene by molecular oxygen over  $\text{Ag}/\text{BaCO}_3^*$  catalyst with Ag crystallite size between 18 nm and 40 nm.

### 3.7. Catalytic reaction mechanism for epoxidation of propylene

To get a knowledge of how Ag crystallite size affected the catalytic performance of  $\text{Ag}/\text{BaCO}_3^*$  catalyst, the temperature-programmed desorption and kinetic experiments of  $\text{Ag}/\text{BaCO}_3^*$  catalysts with different reduction temperatures of HCHO were performed. Fig. 12 and Fig. 13 show temperature-programmed desorption of  $\text{C}_3\text{H}_6$  and  $\text{O}_2$  over  $\text{Ag}/\text{BaCO}_3^*$  catalyst, respectively. As shown in Fig. 12, only a desorption peak of  $\text{C}_3\text{H}_6$  from  $-100^\circ\text{C}$  to  $0^\circ\text{C}$  was observed over  $\text{Ag}/\text{BaCO}_3^*$  catalyst (prepared at the reduction temperature of HCHO of 10 °C and the calcination temperature of 250 °C), which indicated that  $\text{C}_3\text{H}_6$  could not adsorb on the catalyst surface at the reaction temperature of 200 °C and there was very weak interaction between  $\text{C}_3\text{H}_6$  and Ag nanoparticles. Fig. 13 shows  $\text{O}_2$ -TPD profiles of  $\text{Ag}/\text{BaCO}_3^*$  catalysts with different reduc-

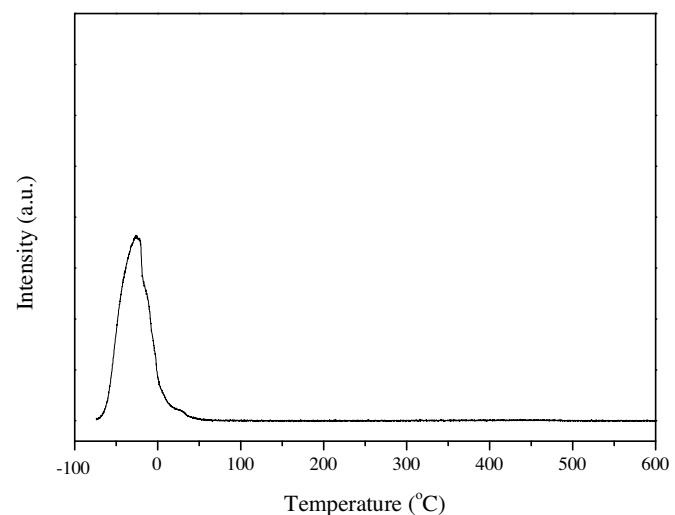


**Fig. 12.**  $\text{C}_3\text{H}_6$ -TPD profile of  $\text{Ag}/\text{BaCO}_3^*$  catalyst at the reduction temperature of HCHO of 10 °C.

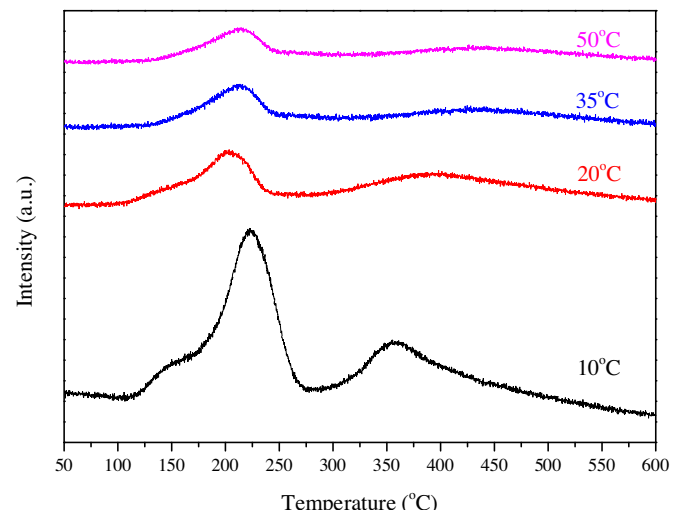


**Fig. 13.**  $\text{O}_2$ -TPD profiles of  $\text{Ag}/\text{BaCO}_3^*$  catalysts with different reduction temperatures of HCHO.

tion temperatures of HCHO. As shown in Fig. 13, the desorption peak of  $\text{O}_2$  was observed from  $100^\circ\text{C}$  to  $250^\circ\text{C}$ , which indicated that  $\text{O}_2$  could adsorb on the catalyst surface at the reaction temperature of 200 °C and there was strong interaction between  $\text{O}_2$  and Ag nanoparticles. Moreover, the  $\text{O}_2$  uptakes decreased significantly with an increase in the reduction temperature of HCHO, which indicated that larger Ag nanoparticles adsorbed fewer oxygen species because of the fewer active sites. As shown in Fig. 13, there were three types of the overlapping peaks of  $\text{O}_2$ -TPD from  $50^\circ\text{C}$  to  $600^\circ\text{C}$ . Based on  $\text{O}_2$ -TPD profiles of an electrolytic silver catalyst reported in the literature [43], these three peaks of  $\text{O}_2$ -TPD were attributed to desorption of three types of oxygen species from the catalyst surface. The peak of  $\text{O}_2$ -TPD at  $150^\circ\text{C}$  was attributed to desorption of a weakly held oxygen species, identified as a state of molecularly chemisorbed oxygen species (nominally superoxo species). The peak of  $\text{O}_2$ -TPD at  $200\text{--}220^\circ\text{C}$  was attributed to desorption of weakly chemisorbed surface atomic oxygen species. The peak of  $\text{O}_2$ -TPD at  $350\text{--}400^\circ\text{C}$  arose from segregation and desorption of bulk-dissolved (subsurface) oxygen species. Because the reaction temperature was  $200^\circ\text{C}$ , we just discussed the former two oxygen species here. The desorption peak of molecular oxygen species gradually disappeared and the desorption peak of atom oxygen

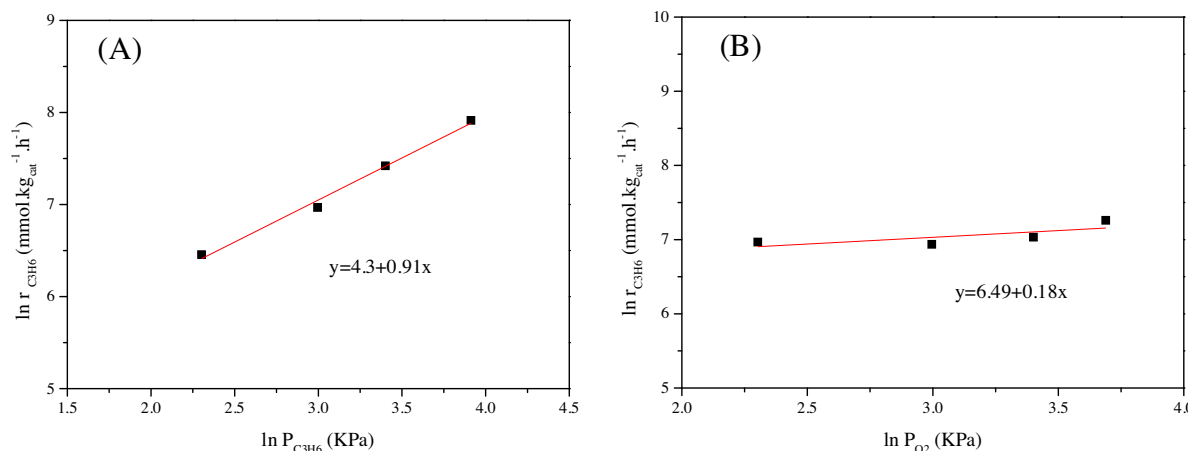


**Fig. 14.** Dependence of the reaction rates of  $C_3H_6$  on the partial pressure of  $C_3H_6$  (A) or the partial pressure of  $O_2$  (B).

species moved to lower temperature with increasing the reduction temperature of HCHO. Therefore molecular oxygen species were probably responsible for epoxidation of propylene to PO by molecular oxygen.

Fig. 14 shows dependence of the reaction rates of  $C_3H_6$  on the partial pressure of  $C_3H_6$  or the partial pressure of  $O_2$  for epoxidation of propylene in a kinetic way. As shown in Fig. 14, the reaction orders of  $C_3H_6$  or  $O_2$  at the reaction temperature of 200 °C over  $Ag/BaCO_3^*$  catalyst were 0.91 or 0.18, approximately 1 and 0, respectively, that was to say,  $r_{C_3H_6} = k_{C_3H_6} \cdot P_{C_3H_6}^{0.91} \cdot P_{O_2}^{0.18} \approx k_{C_3H_6} \cdot P_{C_3H_6}$ . Combined with the results shown in Fig. 12 and Fig. 13, the reaction process was speculated that  $C_3H_6$  in the gas phase reacted with oxygen species already adsorbed on the catalyst surface and followed Rideal–Eley mechanism. This explained why  $Ag/BaCO_3^*$  catalyst of smaller Ag crystallite size with higher  $O_2$  uptakes in  $O_2$ -TPD profile could get higher propylene conversion.

#### 4. Conclusions

$Ag/BaCO_3$ ,  $Ag/BaCO_3^*$  and  $Ag^*/BaCO_3$  catalysts, prepared by the reduction-deposition method, were investigated for gas-phase epoxidation of propylene by molecular oxygen.  $Ag/BaCO_3^*$  catalyst, with pretreatment of  $BaCO_3$  support by ethylene diamine, exhibits better catalytic performance and better durability than  $Ag/BaCO_3$  or  $Ag^*/BaCO_3$  catalysts because of smaller Ag crystallite size.  $O_2$ -TPD experiment shows that carbonaceous species can be oxidized to  $CO_2$  and  $H_2O$  at lower temperature over the deactivated  $Ag/BaCO_3^*$  catalyst with smaller Ag crystallite size. Both lower calcination temperature and lower reduction temperature of HCHO can get smaller Ag crystallite sizes, which is more effective for epoxidation of propylene over  $Ag/BaCO_3^*$  catalyst.  $Ag/BaCO_3^*$  catalyst with the Ag crystallite size of about 18 nm, prepared at the reduction temperature of HCHO of 10 °C and the calcination temperature of 250 °C, achieves 12.5% of propylene conversion and 36.9% of PO selectivity at the reaction temperature of 200 °C. The catalytic reaction mechanism for epoxidation of propylene over  $Ag/BaCO_3^*$  catalyst is that propylene in the gas phase reacts with molecular oxygen species adsorbed on the catalyst surface to produce PO and follows Rideal–Eley mechanism.

#### Acknowledgments

This work was supported by National Basic Research Program of China (2013CB933201), National Natural Science Foundation of China (21577035), and Commission of Science and Technology of Shanghai Municipality (15DZ1205305).

#### References

- [1] T.A. Nijhuis, M. Makkee, J.A. Moulijn, B.M. Weckhuysen, Ind. Eng. Chem. Res. 45 (2006) 3447–3459.
- [2] G. Blanco-Brieva, M.C. Capel-Sánchez, M.P. Frutos, A. Padilla-Polo, J.M. Campos-Martín, J.L.G. Ferro, Ind. Eng. Chem. Res. 47 (2008) 8011–8015.
- [3] T. Hayashi, K. Tanaka, M. Haruta, J. Catal. 178 (1998) 566–575.
- [4] A.K. Sinha, S. Seelan, T. Akita, S. Tsubota, M. Haruta, Appl. Catal. A: Gen. 240 (2003) 243–252.
- [5] J. Chou, E.W. McFarland, Chem. Commun. 14 (2004) 1648–1649.
- [6] J.Q. Lu, X.M. Zhang, J.J. Bravo-Suárez, K.K. Bando, T. Fujitani, S.T. Oyama, J. Catal. 250 (2007) 350–359.
- [7] T. Liu, P. Hacarlioglu, S.T. Oyama, M.F. Luo, X.R. Pan, J.Q. Lu, J. Catal. 267 (2009) 202–206.
- [8] C.H. Liu, Y.J. Guan, E.J.M. Hensen, J.F. Lee, C.M. Yang, J. Catal. 282 (2011) 94–102.
- [9] J.Q. Lu, N. Li, X.R. Pan, C. Zhang, M.F. Luo, Catal. Commun. 28 (2012) 179–182.
- [10] X. Feng, X.Z. Duan, H.Y. Cheng, G. Qian, D. Chen, W.K. Yuan, X.G. Zhou, J. Catal. 325 (2015) 128–135.
- [11] S. Ghosh, S.S. Acharyya, R. Tiwari, B. Sarkar, R.K. Singha, C. Pendem, T. Sasaki, R. Bal, ACS Catal. 4 (2014) 2169–2174.
- [12] L. Cheng, C. Yin, F. Mahmood, B. Liu, J. Greeley, S. Lee, B. Lee, S. Seifert, R.E. Winans, D. Teschner, R. Schlögl, S. Vajda, L.A. Curtiss, ACS Catal. 4 (2014) 32–39.
- [13] X. Yang, S. Kattel, K. Xiong, K. Mudiyanselage, S. Rykov, S.D. Senanayake, J.A. Rodriguez, P. Liu, D.J. Stacioli, L.G. Chen, Angew. Chem. Int. Ed. 54 (2015) 11946–11951.
- [14] W.J. Long, Q.G. Zhai, J.L. He, Q.H. Zhang, W.P. Deng, Y. Wang, ChemPlusChem 77 (2012) 27–30.
- [15] A. Miller, B. Zohour, A. Seubsai, D. Noon, S. Senkan, Ind. Eng. Chem. Res. 52 (2013) 9551–9555.
- [16] A. Seubsai, M. Kahn, B. Zohour, D. Noon, M. Charoenpanich, S. Senkan, Ind. Eng. Chem. Res. 54 (2015) 2638–2645.
- [17] J.L. He, Q.G. Zhai, Q.H. Zhang, W.P. Deng, Y. Wang, J. Catal. 299 (2013) 53–66.
- [18] D. Düzenli, D.O. Atmaca, M.G. Gezer, I. Onal, Appl. Surf. Sci. 355 (2015) 660–666.
- [19] A. Marimuthu, J.W. Zhang, S. Linic, Science 339 (2013) 1590–1593.
- [20] Q. Hua, T. Cao, X.K. Gu, J.Q. Lu, Z.Q. Jiang, X.R. Pan, L.F. Luo, W.X. Li, W.X. Huang, Angew. Chem. Int. Ed. 53 (2014) 4856–4861.
- [21] X. Zheng, Y.L. Guo, Y. Guo, Q. Zhang, X.H. Liu, L. Wang, W.C. Zhan, G.Z. Lu, Rare Metal 34 (2015) 477–490.
- [22] A. Chongterdtoonskul, J.W. Schwank, S. Chavadej, J. Mol. Catal. A: Chem. 372 (2013) 175–182.
- [23] X. Jing, H. Wang, H. Chen, J. Huang, Q. Li, D. Sun, RSC Adv. 4 (2014) 27597–27603.
- [24] W. Diao, C.D. DiGiulio, M.T. Schaal, S. Ma, J.R. Monnier, J. Catal. 322 (2015) 14–23.
- [25] J.Q. Lu, M.F. Luo, H. Lei, C. Li, Appl. Catal. A: Gen. 237 (2002) 11–19.
- [26] J.Q. Lu, J.J. Bravo-Suárez, M. Haruta, S.T. Oyama, Appl. Catal. A: Gen. 302 (2006) 283–295.
- [27] F.W. Zemichael, A. Palermo, M.S. Tikhov, R.M. Lambert, Catal. Lett. 80 (2002) 93–98.
- [28] M.F. Luo, J.Q. Lu, C. Li, Catal. Lett. 86 (2003) 43–49.
- [29] G.J. Jin, G.Z. Lu, Y.L. Guo, Y. Guo, J.S. Wang, X.H. Liu, Catal. Today 93–95 (2004) 173–182.
- [30] W. Yao, G.Z. Lu, Y.L. Guo, Y. Guo, Y.S. Wang, Z.G. Zhang, J. Mol. Catal. A: Chem. 276 (2007) 162–167.
- [31] X. Zheng, Q. Zhang, Y.L. Guo, W.C. Zhan, Y. Guo, Y.S. Wang, G.Z. Lu, J. Mol. Catal. A: Chem. 357 (2012) 106–111.

- [32] J.Q. Lu, J.J. Bravo-Suárez, A. Takahashi, M. Haruta, S.T. Oyama, *J. Catal.* 232 (2005) 85–95.
- [33] L.M. Molina, S. Lee, K. Sell, G. Barcaro, A. Fortunelli, B. Lee, S. Seifert, R.E. Winans, J.W. Elam, M.J. Pellin, I. Barke, V.V. Oeynhausen, Y. Lei, R.J. Meyer, J.A. Alonso, A.F. Rodríguez, A. Kleibert, S. Giorgio, C.R. Henry, K.H. Meiwes-Broer, S. Vajda, *Catal. Today* 160 (2011) 116–130.
- [34] Y. Lei, F. Mahmood, S. Lee, J. Greeley, B. Lee, S. Seifert, R.E. Winans, J.W. Elam, R.J. Meyer, P.C. Redfern, D. Teschner, R. Schlägl, M.J. Pellin, L.A. Curtiss, S. Vajda, *Science* 328 (2010) 224–228.
- [35] M. Boronat, A. Pulido, P. Concepción, A. Corma, *Phys. Chem. Chem. Phys.* 16 (2014) 26600–26612.
- [36] L.B. Yu, Y.Y. Shi, Z. Zhao, H.B. Yin, Y.C. Wei, J. Liu, W.B. Kang, T.S. Jiang, A.L. Wang, *Catal. Commun.* 12 (2011) 616–620.
- [37] L. Yang, J.H. Chen, X.G. Wei, B. Liu, Y.F. Kuang, *Electrochim. Acta* 53 (2007) 777–784.
- [38] A.Q. Wang, X.Y. Liu, C.Y. Mou, T. Zhang, *J. Catal.* 308 (2013) 258–271.
- [39] A.G. Bhavani, W.Y. Kim, J.W. Lee, J.S. Lee, *ChemCatChem* 7 (2015) 1445–1452.
- [40] N. Nojiri, Y. Sakai, Silver catalyst for production of ethylene oxide from ethylene [P]. US 4786624 (1988).
- [41] A.A. Herzing, C.J. Kiely, A.F. Carley, P. Landon, G.J. Hutchings, *Science* 321 (2008) 1331–1335.
- [42] S.R. Challa, A.T. Delariva, T.W. Hansen, S. Helveg, J. Sehested, P.L. Hansen, F. Garzon, A.K. Datye, *J. Am. Chem. Soc.* 133 (2011) 20672–20675.
- [43] G.I.N. Waterhouse, G.A. Bowmaker, J.B. Metson, *Appl. Surf. Sci.* 214 (2003) 36–51.